HHS Public Access

Author manuscript

J Inorg Biochem. Author manuscript; available in PMC 2017 May 01.

Published in final edited form as:

J Inorg Biochem. 2016 May ; 158: 62–69. doi:10.1016/j.jinorgbio.2015.12.025.

Disruption of a Hydrogen Bond Network in Human versus Spider Monkey Cytochrome *c* Affects Heme Crevice Stability

Matthew E. Goldes[a], **Margaret E. Jeakins-Cooley**[a], **Levi J. McClelland**[a,b], **Tung-Chung Mou**[b,c], and **Bruce E. Bowler**[*,a,c]

[a]Department of Chemistry and Biochemistry, University of Montana, Missoula, MT 59812

[b]Division of Biological Sciences, University of Montana, Missoula, MT 59812

[c]Center for Biomolecular Structure and Dynamics, University of Montana, Missoula, MT 59812

Abstract

The hypothesis that the recent rapid evolution of primate cytochromes *c*, which primarily involves residues in the least stable Ω-loop (Ω-loop C, residues 40 – 57), stabilizes the heme crevice of cytochrome *c* relative to other mammals, is tested. To accomplish this goal, we have compared the properties of human and spider monkey cytochrome *c* and a set of four variants produced in the process of converting human cytochrome *c* into spider monkey cytochrome *c*. The global stability of all variants has been measured by guanidine hydrochloride denaturation. The stability of the heme crevice has been assessed with the alkaline conformational transition. Structural insight into the effects of the five amino acid substitutions needed to convert human cytochrome *c* into spider monkey cytochrome *c* is provide by a 1.15 Å resolution structure of spider monkey cytochrome *c*. The global stability for all variants is near 9.0 kcal/mol at 25 °C and pH 7, which is higher than that observed for other mammalian cytochromes *c*. The heme crevice stability is more sensitive to the substitutions required to produce spider monkey cytochrome *c* with decreases of up to 0.5 units in the apparent pK_a of the alkaline conformational transition relative to human cytochrome *c*. The structure of spider monkey cytochrome *c* indicates that the Y46F substitution destabilizes the heme crevice by disrupting an extensive hydrogen bond network that connects three surface loops including Ω-loop D (residues 70–85), which contains the Met80 heme ligand.

Graphical Abstract

Destabilization of the heme crevice during the rapid evolution of primate cytochromes *c* is primarily due to a Y46F substitution, which disrupts of a hydrogen bond network that knits together three surface Ω-loops.

[*]Corresponding Author. Tel.: +406 2436114; fax: +406 2434227. ; Email: bruce.bowler@umontana.edu (B. E. Bowler)

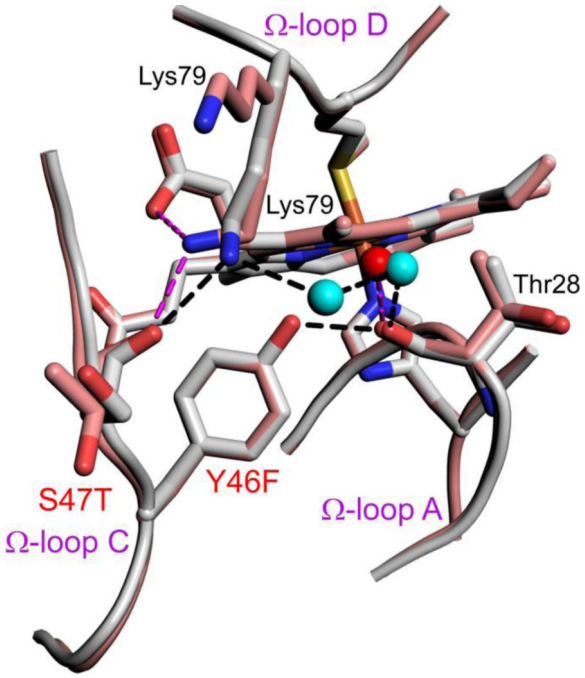

Keywords

Spider Monkey Cytochrome *c*; Global stability; Alkaline conformational transition; Heme crevice stability; Hydrogen bond network

1. Introduction

Cytochrome *c* (Cyt*c*) resides in the intermembrane space of mitochondria. Its function as a component of the electron transport chain has been known for many years [1, 2]. About 20 years ago, it was discovered that release of Cyt*c* from mitochondria, followed by its interaction with Apaf-1 to form the apoptosome [3, 4], is a critical signaling event in the intrinsic pathway of apoptosis [5, 6]. Furthermore, peroxidative activity, particularly directed at the inner mitochondrial membrane lipid, cardiolipin (CL), is believed to be the earliest signal in the intrinsic pathway of apoptosis [7]. More recently it has been postulated that the peroxidase activity of Cyt*c* may provide a rich source of CL-based lipid signaling agents [8, 9]. The peroxidase activity of Cyt*c* is linked to loss of the Met80-heme bond [5, 6]. Thus, there has been considerable interest recently in the factors that control the stability of the heme crevice [10, 11].

It has been noted recently that there has been a rapid evolution of Cyt*c* in the primate lineage [12, 13]. It has been postulated that this evolution may be coupled to evolution of cytochrome *c* oxidase. However, many of the mutations in the evolution of primate cytochromes *c* are found in a surface loop, Ω-loop C (residues 40–57), which is believed to modulate the opening of the heme crevice in the alkaline conformational transition [14]. Human Cyt*c* (Hu Cyt*c*) and spider monkey Cyt*c* (SM Cyt*c*) are on different branches of the evolutionary tree of primate cytochromes *c*. Furthermore, it has been postulated that the

A50E substitution, found in SM Cyt*c* relative Hu Cyt*c*, may destabilize the heme crevice by providing an electrostatic interaction that can compete with the hydrogen bond between the ε-amino group of Lys79 and the main chain carbonyl of residue 47 [15].

As an initial test of the hypothesis that the rapid evolution of primate cytochromes *c* may also affect the stability of the heme crevice and thus could be important for the peroxidase activity of Cyt*c* in apoptosis, we have prepared SM Cyt*c* from Hu Cyt*c* in a stepwise manner. There are only five substitutions in the sequence of SM Cyt*c* relative to Hu Cyt*c* [15]. However, four of these substitutions are in Ω-loop C. Here, we characterize the global stability of Hu Cyt*c*, SM Cyt*c* and the four intermediate variants used to produce SM Cyt*c* from Hu Cyt*c*. To characterize the effects of these substitutions on the stability of the heme crevice, we have measured the alkaline conformational transition of the set of six cytochromes *c*. We also report a 1.15 Å structure of SM Cyt*c* that provides high resolution structural insight into the effects of these mutations on heme crevice stability.

We find that the effects of the five substitutions required to produce SM Cyt*c* from Hu Cyt*c* on the global stability of Cyt*c* are modest. However, the apparent pK_a of the alkaline transition is decreased by up to 0.5 units. The Y46F mutation has the largest effect on the alkaline transition. This observation is supported by comparison of our SM Cyt*c* structure with that of Hu Cyt*c*, which shows that the Y46F mutation compromises the integrity a hydrogen bond network that holds together three surface loops in the structure of Cyt*c*.

2. Experimentals

2.1. Preparation of the spider monkey cytochrome c expression vector

The pBTR(HumanCc) plasmid for expression of Hu Cyt*c* in *Escherichia coli* was provided by Gary Pielak at the University of North Carolina [3]. The pBTR(HumanCc) plasmid is a derivative of the pBTR1 plasmid [16, 17] produced by replacing the yeast iso-1-Cyt*c* gene (CYC1) with a synthetic Hu Cyt*c* gene [3, 18]. Thus, the plasmid co-expresses the yeast heme lyase gene (CYC3) permitting covalent attachment of heme in the cytoplasm of *E. coli*. SM Cyt*c* differs at five sequence positions from Hu Cyt*c* [15]. The necessary K8R, P44S, Y46F, S47T and A50E mutations were introduced sequentially starting at the N-terminus of the protein using the QuikChange PCR-based mutagenesis protocol (Agilent) producing the set of variants K8R, K8R/P44S, K8R/P44S/Y46F, K8R/P44S/Y46F/S47T and finally SM Cyt*c* (K8R/P44S/Y46F/S47T/A50E). The final SM Cyt*c* plasmid pBTR(SMCyt*c*) is available through Addgene (https://www.addgene.org/). Primers used for mutagenesis are listed in Table S1 of the Supplementary Data. Plasmid DNA for each variant was prepared from TG-1 *E. coli* cells transformed with DNA produced by the QuikChange protocol using the Qiagen miniprep procedure (Qiagen). The entire coding region of the Cyt*c* gene was sequenced at the Murdock DNA Sequencing facility at the University of Montana to confirm the identity of each variant.

2.2. Expression of Cytc variants

Cyt*c* variants were expressed after transformation of the expression plasmid into competent *E. coli* BL21 DE3 cells (EdgeBio). Transformed cells on agar plates were re-suspended in

sterile L-broth (4 mL) and used to inoculate 1 L of sterilize 2xYT broth (1 L deionized H_2O, 16 g tryptone, 10 g yeast extract, 5 g NaCl) in a Fernbach flask. 2 mL of sterile ampicillin (100 mg/mL) was added to each flask. All flasks were grown in an orbital shaker incubator (Thermo Forma 435) at 30 °C or 37 °C for 24 h.

After growth, the cells were pelleted using a Sorvall RC 5C+ centrifuge (Thermo) with a GS3 rotor (5,000 rpm) and stored at −80 °C. Protein was isolated from cell pellets using methods similar to those reported for yeast iso-1-cytochrome *c* (iso-1-Cyt*c*) [19]. In brief, before mechanically lysing the cells, they were subjected to three freeze-thaw cycles at −80 °C (3 h) and 4 °C (2 h), respectively. Cell pellets were then re-suspended in 2 mL of lysis buffer (100 mM Tris, 1 mM NaEDTA, 500 mM NaCl, pH 8.0) per gram of cells. A small amount of lyophilized DNase and RNase powder was added along with the protease inhibitor PMSF to a final concentration of 3 mM. The resuspended cells were then passed through a French Pressure Cell (SLM Aminco) a minimum of four times. The lysed cells were spun down at 10,000 rpm (GSA rotor) in a Sorvall RC 5C+ centrifuge for 30 min and the supernatant was passed through a filter cloth. The supernatant was brought to 50% saturation with ammonium sulfate and stirred overnight at 4 °C, followed by centrifugation at 10,000 rpm (GSA rotor) to remove precipitated protein impurities. The supernatant was passed through filter cloth and dialyzed against 12.5 mM sodium phosphate, pH 7.2, 1.0 mM EDTA, 2.0 mM β-mercaptoethanol. The dialyzed protein was batch loaded onto CM Sepharose fast-flow beads (GE Healthcare) and the resin packed into glass column (3.2 cm × 18.4 cm) followed by elution of Cyt*c* with a 200 mL linear gradient from 0 to 0.8 M NaCl in 50 mM sodium phosphate, pH 7.2, 1mM EDTA, 2 mM β-mercaptoethanol. Cyt*c* containing fractions were exchanged into 50 mM sodium phosphate at pH 7 (HPLC buffer A) using an Amicon stirred ultrafiltration cell and then concentrated to ~1.6 mg/mL using centrifuge ultrafiltration. Aliquots of 1.5 mL were flash frozen and stored at −80°C freezer for later use. Yields of SM Cyt*c* are 9 – 10 mg per liter of 2x YT culture.

Aliquots were thawed and purified by HPLC using a Bio-Rad UNO S6 column immediately in advance of experiments. The following gradient at a flow rate of 3.0 mL/min was used for purification: 0 % B from 0 to 7 min, increase to 30 % B from 7 to 34 min, maintain 30 % B from 34 to 40 min., increase to 100 % B from 40 to 43 min, maintain 100 % B from 43 to 50 min, decrease to 0 % B from 50 to 53 min, maintain 0 % B from 53 to 63 min. HPLC buffer B is HPLC buffer A with 1.0 M NaCl. Pure Cyt*c* fractions were concentrated by ultrafiltration.

The molecular weight of the SM Cyt*c* was measured to be 12,307.7 g/mol ($M+H^+$, expected $M+H^+$ = 12,309.1 g/mol) using a Bruker microflex MALDI-ToF mass spectrometer. Protein Calibration Standard I (Bruker Part No. 206355) was used to calibrate the mass spectrometer.

2.3 Oxidization of Cytc

All experiments were performed on the oxidized state, Fe(III)heme, of Cyt*c*. Potassium ferricyanide was used to oxidize the protein using 5 mg of ferricyanide per mg of protein. After 15 min at 4 °C, the Cyt*c* solution was spun in a microcentrifuge for 5 min and loaded

on a column packed with Sephadex G-25 superfine size-exclusion resin. The sephadex G-25 resin was equilibrated and run with the buffer to be used in the experiment.

2.4 Measurement of global stability by guanidine hydrochloride denaturation

Circular dichroism (CD) spectroscopy was used to monitor guanidine hydrochloride (GdnHCl) unfolding of Cyt*c* variants. A 4 μM Cyt*c* sample was prepared in CD Buffer (20 mM Tris, 40 mM NaCl adjusted to pH 7.0). A 6 M GdnHCl solution in CD Buffer, also containing 4 μM Cyt*c*, was used to titrate the Cyt*c* sample in CD buffer. Titrations were carried out at 25 °C using a Hamilton Microlab 500 titrator interfaced with an Applied Photophysics Chirascan CD spectrophotometer. Data were collected at 222 nm using 250 nm as background to account for instrumental drift during the titration.

Plots of background corrected ellipticity at 222 nm, $\theta_{222corr}$ ($\theta_{222corr} = \theta_{222} - \theta_{250}$), versus GdnHCl concentration were fit to a linear free energy relationship between the free energy of unfolding, ΔG_u, and GdnHCl concentration using nonlinear least squares methods (SigmaPlot 7), and Eq. (1) [20], where θ_N is the ellipticity of the native state of Cyt*c*, θ_D is the ellipticity of the

$$\theta_{222\mathrm{corr}} = \frac{\theta_N + \left[(\theta_D + m_D[\mathrm{GdnHCl}])\exp\left\{\frac{m[\mathrm{GdnHCl}] - \Delta G_u^\circ(H_2O)}{RT}\right\}\right]}{1 + \exp\left\{\frac{m[\mathrm{GdnHCl}] - \Delta G_u^\circ(H_2O)}{RT}\right\}} \quad (1)$$

denatured state extrapolated to 0 M GdnHCl, m_D is the slope of the denatured state baseline as a function of GdnHCl concentration, $\Delta G_u°(H_2O)$ is ΔG_u extrapolated to 0 M GdnHCl and m is the slope of ΔG_u as a function GdnHCl concentration.

2.5 Measurement of local stability via the alkaline conformational transition

The alkaline conformation transition of the Cyt*c* variants was measured by pH titration monitored at 695 nm, an absorbance band sensitive to Met80-hemeFe(III) ligation [2, 21, 22]. A 400 μM protein in 200 mM NaCl solution (2x-stock) was mixed 1:1 with deionized water to make the titration solution (200 μM Cyt*c* in 100 mM NaCl). An equal volume of HCl solution and the 2x-stock was added to adjust the titration solution to about pH 6.3. For each step of the titration, equal volumes of an NaOH solution of appropriate concentration and of the 2x-stock solution were added to raise the pH of the titration solution by 0.15–0.20 pH units. The pH was recorded with a semimicro calomel electrode and the spectrum was recorded from 750 to 500 nm at each step. The titration was continued until a pH of 11 was achieved. Titrations were carried out at room temperature, 23 ± 1 °C.

The absorbance at 750 nm, A_{750}, was subtracted from the absorbance at 695 nm, A_{695}, to correct for instrumental drift during the titration. The corrected absorbance at 695 nm, $A_{695corr}$ ($A_{695corr} = A_{695} - A_{750}$), was plotted against pH and fit to a modified form of the Henderson-Hasselbalch equation, Eq. (2), which accounts for the number of protons linked to the alkaline transition, *n*.

$$A_{695corr} = \frac{A_N + A_{alk} \times 10^{n(pK_{app} - pH)}}{1 + 10^{n(pK_{app} - pH)}} \quad (2)$$

Fits were carried out using nonlinear least squares methods (SigmaPlot 7) yielding, n and the apparent pK_a, pK_{app}, of the alkaline conformational transition.

2.6 Ionic strength dependence of the alkaline conformational transition of SM Cytc

The methods of Osheroff et al. [15] were used to carry out measurement of the alkaline conformational transition as a function of ionic strength. A 25 mM Tris/acetate buffer, pH 7.0, stock buffer was prepared by titrating acetic acid with 1 M Tris base solution until a pH of 7 was achieved. The buffer was adjusted to its final volume in a volumetric flask such that the concentration of acetate was 25 mM. For pH titrations with NaOH, each $TrisH^+$ titrated by NaOH is replace by Na^+, so the ionic strength does not change with pH. This buffer was diluted to 10 mM for oxidation of SM Cyt*c* and separation of oxidized protein from ferricyanide by Sephadex G25 chromatography. To increase the ionic strength of the solution, NaCl was added to create the desired solution ionic strength. Titrations were carried out and data were analyzed as described in section 2.5.

2.7. Crystallization, data collection, and structure determination of SM Cytc

The isolated SM Cyt*c* protein was concentrated to 37 mg/ml by centrifuge ultrafiltration in a buffer of 50 mM Tris·HCl, pH 7. The initial crystallization condition was obtained by commercial crystallization screening trials. Additional vapor diffusion crystallization experiments were set up in grid screening by expanding the pH range and precipitant concentrations in 24-well VDX plates. After 2 to 4 weeks of equilibration at 20 °C, large cubic-shaped crystals were obtained by mixing 1 μL of protein with an equal volume of 0.1 M LiCl, 20% PEG 6000, 0.1 M HEPES sodium salt, pH 8.2, reservoir solution. For cryoprotection, crystals were transferred into reservoir solution containing 30% (v/v) PEG 400 and flash-frozen in a 100 K nitrogen gas stream.

Diffraction data were collected at the Stanford Synchrotron Radiation Lightsource SSRL-SMB 14-1 beamline using a MAR325 CCD detector at an incident beam wavelength of 1.22 Å. Images were indexed, integrated, and scaled using HKL2000 [23]. The initial phasing map was determined by molecular replacement with Phaser, integrated in the PHENIX software suite [24], using the coordinates of yeast iso-1-Cyt*c* (PDB 2YCC) as a search model, against 8 to 2 Å experimental data. A continuous electron density map with a clearly defined protein-solvent boundary was observed. The initial model was first subjected to one cycle of rigid-body refinement using PHENIX. Subsequently, the model was further refined by iterative model rebuilding with COOT [25] and refinement of atomic positions, real space, occupancy, and isotropic B-factor parameters with PHENIX using a subset of reflections for calculation of R_{free} (Table 1). At a later stage of refinement, the refined structure was improved to a final resolution of 1.15 Å and the coordinates of hydrogen atoms were included in the subsequent refinement cycles. Data collection and refinement statistics of the final model are shown in Table 1. The coordinates and structure factors for

spider monkey Cyt*c* have been deposited in the Protein Data Bank (PDB) under the ID code: 5DFS.

3. Results and Discussion

3.1 Global Stability of Human and Spider Monkey Cytc

Spider monkey cytochrome *c*, SM Cyt*c*, has five substitutions relative to Human Cyt*c*, Hu Cyt*c*. Most of these substitutions occur in the Ω-loop that runs from residues 40 to 57 (Ω-loop C). The sole substitution outside of this region is in the N-terminal helix, a K8R substitution. We made this conservative mutation first expecting that its effect on stability would be modest. The remaining four substitutions occur in a short sequence segment from residues 44 to 50. Based on native-state hydrogen-deuterium exchange (NSHX) studies on equine Cyt*c* and limited proteolysis on yeast iso-1-Cyt*c*, this Ω-loop is the least stable part of mitochondrial Cyt*c* [26, 27]. Thus, changes in stability are expected to propagate upward affecting the global stability of Hu Cyt*c* versus SM Cyt*c* [28, 29]. Mutations were made sequentially starting at position 44 and ending with the position 50 substitution (A50E).

To assess the effect of each mutation on global stability we carried out GdnHCl denaturation of each protein. The unfolding titration curves for Hu Cyt, SM Cytc and the four intervening variants are shown in Fig. 1. It is evident from the GdnHCl denaturation data that the unfolding midpoint concentration, C_m, for all six sequence variants of Cyt*c* is similar. The $\Delta G_u°(H_2O)$ of 8.9 ± 0.2 kcal/mol (Table 2) that we observe for the Hu Cyt*c*, is similar to global stability of ~ 8.7 kcal/mol at 298 K reported for Hu Cyt*c* based on thermal denaturation data [3]. Our GdnHCl data also indicate that Hu Cyt*c* is more stable that equine or bovine Cyt*c* as determined by GdnHCl denaturation methods (Table 2). Thermal denaturation data also show that Hu Cyt*c* is more stable than equine Cyt*c* (stability ~6.6 kcal/mol at 298 K, see ref. [3]). Table 2 shows that SM Cyt*c* and the set of variants used to produce SM Cyt*c* from Hu Cyt*c* all have global stability similar to Hu Cyt*c*.

Hu Cyt*c* and SM Cyt*c* and the set of variants used to convert Hu Cyt*c* to SM Cyt*c* also have similar denaturant *m*-values of ~3.5 kcal $mol^{-1}M^{-1}$. These values are higher than observed for equine and bovine Cyt*c* but smaller than observed for yeast iso-1-Cyt*c*. Analysis of the denaturant dependence of the stability of the substructures of equine Cyt*c* derived from NSHX studies shows that there is a significant population of intermediates in the transition region for GdnHCl unfolding of equine Cyt*c* [30]. The lower GdnHCl *m*-value for equine Cyt*c* (Table 1, see ref [31]) versus Hu and SM Cyt*c* is consistent with a greater population of intermediates during global unfolding of equine Cyt*c* than for primate cytochromes *c*. Limited proteolysis studies on yeast iso-1-Cyt*c* show that the least stable substructure is close to the global stability of iso-1-Cyt*c* [27]. The *m*-value of iso-1-Cyt*c* [32] is larger than for Hu and SM Cyt*c*, indicating that population of intermediates is less during global unfolding of yeast than for the primate cytochromes *c*. Thus, the intermediate magnitude of the *m*-value for Hu and SM Cyt*c* relative to equine and yeast suggests that the free energy required to unfold the least stable substructure of Hu and SM Cyt*c* is greater than for equine Cyt*c*.

3.2 Alkaline conformational transition of Hu and SM Cytc

The alkaline conformational transition of oxidized, Fe(III)heme, Cyt*c* occurs at mildly alkaline pH [2, 33]. It involves replacement of the native state heme ligand, Met80, with lysine side chains from Ω-loop D (residues 70–85), altering the structure of this Ω-loop [34, 35]. The alkaline conformational transition correlates well with the stability of the unstable substructure of Cyt*c* corresponding to Ω-loop D [36] and thus is often used as a proxy for the stability of the heme crevice. Hydrogen exchange methods indicate that the rate of the alkaline conformational transition is limited by opening of Ω-loop C (residues 40–57) the least stable substructure of mitochondrial cytochromes *c* [26, 27]. Thus, the substitutions in this region required to convert Hu to SM Cyt*c* might be expected to affect the alkaline conformational transition.

Fig. 2 shows that, unlike global stability, the local stability of Ω-loop D is sensitive to mutations in Ω-loop C. The magnitude of pK_{app} for Hu Cyt*c* and the K8R and K8R/P44S variants is within error unchanged (Table 3). However, addition of the Y46F mutation leads to a significant decrease of 0.4 units in pK_{app} relative to Hu Cyt*c*. There is a small additional decrease in pK_{app} when the S47T mutation is added. The combined effect these two mutations leads to a destabilization of 0.66 kcal/mol of the native state of Hu Cyt*c* relative to its alkaline conformer. The final mutation (A50E), producing SM Cyt*c*, partially reverses the destabilizing effect of the Y46F and S47T mutations on the native state relative to the alkaline state of Cyt*c*. Thus, the net destabilization of the native state relative to the alkaline state for SM versus Hu Cyt*c* is only ~0.3 kcal/mol ($\Delta\Delta G_{alk} = ln(10)RT\Delta pK_{app}$).

There are a number of measurements of the pK_{app} for the alkaline conformational transition of Hu Cyt*c* available in the literature. Margoliash and coworkers reported the pK_{app} of Hu Cyt*c* isolated from human heart (with N-terminal acetylation) as 9.50 at 10 mM ionic strength rising to 9.85 at 250 and 500 mM ionic strength. Our pK_{app} of 9.54 obtained at ~100 mM ionic strength falls in the middle of this range as would be expected. Under similar conditions, equine Cyt*c* has a pK_{app} ~ 0.4 to 0.45 units lower [15]. Thus, the lower global stability of equine Cyt*c* relative to Hu Cyt*c* is correlated with lower stability of the heme crevice as measured by the alkaline conformational transition. Other reported values for the pK_{app} of Hu Cyt*c* are for *E. coli*-expressed Hu Cyt*c* (not N-terminally acetylated) and range from 9.0 to 9.9 [37–41]. The pK_{app} of Cyt*c* is sensitive to ionic strength and specific ion interactions [15, 42, 43]. Some of this observed range likely results from specific anion binding effects due to phosphate and citrate in the titration buffers used.

For Hu Cyt*c*, the pK_{app} for a Y46F variant has been reported. Relative to the value reported for Hu Cyt*c*, the pK_{app} decreases by ~0.6 units for the Y46F variant, similar the ~0.4 unit decrease in pK_{app} we observe when the Y46F mutation is added to the K8R/P44S variant (Table 3).

Hu Cyt*c* and the K8R and K8R/P44S all have alkaline conformational transitions consistent with the release of a single proton ($n = 1$, see Table 3) being linked to the conformational change. After addition of the Y46F mutation, n drops to ~0.9. The decrease in n may reflect a change in coupling of protonation equilibria to the alkaline conformational transition, which have been shown to be complex in this pH regime [44–46]. It may also reflect

mutation-induced changes in the pK_a of one of the lysine ligands contributing to the alkaline state leading to a broadening of the transition [47, 48].

3.3 Ionic strength dependence of pK$_{app}$

The pK_{app} of 9.32 ± 0.03 we observed for SM Cyt*c* in 0.1 M NaCl is similar to the pK_{app} of 9.3 observed by Margoliash and coworkers in the presence of 0.25 M sodium acetate [15]. However, at low ionic strength (10 mM Tris acetate pH 7) the pK_{app} observed by Margoliash and coworkers decreased to 8.70 [15]. They proposed that the large decrease in the pK_{app} observed for SM Cyt*c* was due to an electrostatic interaction between Glu50 and Lys79 competing with the heme crevice stabilizing hydrogen bond between the carbonyl-O of residue 47 and the ε-amino group of Lys79. The observation that the A50E mutation partially reverses the effect of the Y46F and S47T mutations appears at odds with this proposal. Therefore, we studied the ionic strength dependence of the pK_{app} of SM Cyt*c*.

In 10 mM Tris acetate, we find that the pK_{app} of *E. coli*-expressed SM Cyt*c* is similar to that observed in 100 mM NaCl and about 0.5 units higher that observed for SM Cyt*c* obtained from its natural source (Table 4). Addition of NaCl to 10 mM Tris acetate to raise the ionic strength to 50 mM and 250 mM has only modest effects on the pK_{app}. The large difference in the pK_{app} in 10 mM Tris acetate for SM Cyt*c* expressed from *E. coli* versus from its natural source, points to the N-terminal acetylation of SM Cyt*c* from its native source as a possible cause for the observed difference.

It has been shown that phosphate, but not acetate, can strongly increase the intensity of the 695 nm absorbance band suggesting that phosphate can strengthen the heme-Met80 bond [49]. While acetate binds only weakly to cytochrome *c* [42], both phosphate and chloride [50] bind specifically. Thus, as a control experiment the effect of increasing Cl^- concentration on the 695 nm absorbance band of SM Cyt*c* was monitored. In contrast to phosphate binding to horse Cyt*c* [49], no significant effect is observed from 0 to 250 mM Cl^- on the magnitude of the extinction coefficient at 695 nm (Fig. S1). Thus, Cl^- does not appear to directly affect the strength of the heme-Met80 bond for SM Cyt*c*.

Interestingly, there is a drop in the number of protons, *n*, linked to the alkaline conformational transition at ionic strengths of 10 mM and 50 mM by ~0.1 relative to the *n* observed in 100 mM NaCl and at an ionic strength of 250 mM (Tables 3 and 4). It has also been shown that the alkaline transition is less cooperative at low ionic strength for horse Cyt*c* [45]. Loss of cooperativity can be achieved if the alkaline transition involves two ionizable ligands, where one of the ionizable ligands has a significantly lower pK_a than the other ligand but does not drive the alkaline transition to completion [51]. Fig. S2 demonstrates that an equally good fit to the data as with Eq. (2) can be achieved at low ionic strength with this model assuming that there are two lysine ligands for the alkaline state with significantly different pK_a values [47]. The N-terminal amino group of *E. coli*-expressed horse Cyt*c* can participate in the alkaline conformational transition [36]. Thus, we cannot rule out the N-terminal amino group as a ligand in the alkaline state.

3.4 High resolution X-ray structure of SM Cytc

To gain insight into the differences in the alkaline conformational transition between Hu Cyt*c* and SM Cyt*c* we prepared crystals of SM Cyt*c*. The crystals diffracted to 1.15 Å resolution providing a high quality structural model for SM Cyt*c* (R_{work} = 0.159; R_{free} = 0.182; see Table 1). Fig. 3 shows the electron density around the heme including the hydrogen bonding network that includes Tyr67, Asn52, Thr78 and a buried water molecule, showing the high quality of the electron density map and its fit to the model. There are two molecules of SM Cyt*c* (chains A and B) in the asymmetric unit, which align with a C_α RMS deviation of 0.385 Å. There are different conformers for 17 side chains in the two molecules of the asymmetric unit. Most of these are at solvent exposed sites. Two side chains in chain A and four in chain B were fit to two rotamers. Only Arg91 has two rotamers in both chains. Several of these alternate side chain conformers will be highlighted in the discussion that follows.

Buried water molecules are characteristic of mitochondrial cytochromes *c* [52]. There are three buried water molecules in chain A and six in chain B. Two of the additional buried waters in chain B are near the surface and result from alternate conformers of the His33 and Asn103 side chains in chain A versus B. One buried water molecule (B-factor = 10.35 $Å^2$, chain A) is hydrogen bonded to Asn52, Tyr67 and Thr78 and is observed for both chains (Fig. 3 and Fig. 4). This water has been implicated in redox function [52, 53]. A second buried water molecule (B-factor = 10.84 $Å^2$, chain A) is hydrogen bonded to heme propionate A, main chain atoms of Lys39 and Gln42 and the side chain of Arg38 (Fig. 4). This water is believed to be important for holding Arg38 against the heme, allowing Arg38 to regulate the heme redox potential by charge-charge interactions [54]. Recent structural studies on an alternate conformer of K72A iso-1-Cyt*c* show that the Arg38 side chain can gate access of water to the heme crevice, perhaps mediating general acid/base catalysis during peroxidase activity associated with apoptosis [11]. These two buried waters are broadly conserved in mitochondrial cytochromes *c* and as indicated above may be important for function [52, 53]. A third buried water (B-factor = 9.29 $Å^2$, chain A) hydrogen bonded to main atoms of Thr19, Lys25, Lys27, and Gly29 and the side chain of Thr19 sits near the heme ligand His18 and may help to stabilize a tight turn [55]. The remaining buried water is only observed in chain B and is hydrogen bonded to heme propionate A, the main chain of Asn31 and the side of Arg38. This water is observed in yeast iso-1-Cyt*c* [52, 56, 57], but not in horse [53, 55] and human [41] Cyt*c* (Fig. S3).

As can be seen in Fig. 4, the structures of SM Cyt*c* and Hu Cyt*c* overlay well (C_α RMSD of 0.390 Å, chain A versus chain A). The main chain overlays nearly perfectly with small deviations near the P44S substitution, in the single turn of helix running from residues 49 to 56 and near Gly77 in Ω-loop D. The rotamers of the side chains at the positions of the substituted side chains P44S (in chain B a different rotamer is observed, Fig. S3), Y46F and S47T are surprisingly similar. The surface substitutions, K8R and A50E, have similar C_β positions. The small main chain deviation in the short 50's helix leads to an alternate rotamer for Asn52 (Fig. 4) that significantly lengthens the hydrogen bonds to the buried water adjacent to Met80 relative to those observed in chain B where the same rotamer of Asn52 as for Hu Cyt*c* is observed (Fig. 4 versus Fig. S3). For chain B of SM Cyt*c*, the main

chain deviations near the P44S substitution are smaller relative to Hu Cyt*c*, and similar in the short 50's helix. However, the displacement of Ω-loop D in chain B of SM Cyt*c* relative to Hu Cyt*c* occurs primarily after Met80 (Fig. S3). Thus, while different in detail, both molecules of SM Cyt*c*, show structural deviations that might affect the stability of Ω-loop D.

The A50E mutation has been proposed to provide an electrostatic interaction with Lys79 which competes with a hydrogen bond from the ε-amino group of Lys79 to the main chain carbonyl of residue 47. This hydrogen bond is believed to stabilize the heme crevice and thus the A50E mutation in SM Cyt*c* is believed to explain the low pK_{app} for SM Cyt*c* relative to Hu Cyt*c*. Our structural data show that Glu50 forms an electrostatic contact with Lys53 (Fig. 4). Thus, the effect of the A50E mutation on heme crevice stability may be only indirect, leading instead to subtle adjustments to the main chain of the 50's helix as described above.

The Y46F mutation introduces the largest decrease in the pK_{app} of the alkaline transition as Hu Cyt*c* is converted toward SM Cyt*c* (Table 2). In Hu Cyt*c*, Tyr46 is part of a hydrogen bond network that knits together three different surface Ω-loops (Fig. 5). The hydroxyl group of Tyr46 is hydrogen bonded to the carbonyl-O of Thr28. The ε-amino group of Lys79 is hydrogen bonded to the main chain carbonyl-O of Ser47 and to the Thr28 carbonyl-O through two bridging water molecules. In SM Cyt*c*, the Y46F substitution causes loss of the hydrogen bond to the Thr28 carbonyl-O. Loss of this contact destabilizes the Lys79 ε-amino group to Thr28 carbonyl-O water-bridge causing Lys79 to adopt two conformations in chain A (Fig. 5). In one conformer (44% occupancy), the Lys79 ε-amino group to Thr47 carbonyl-O interaction is maintained and a new hydrogen bond to heme propionate D is formed. In the other conformer (56% occupancy), Lys79 projects into the solvent. In Chain B of SM Cyt*c*, the conformation of Lys79 is similar to that in Hu Cyt*c*. However, loss of the Tyr46 hydroxyl to Thr28 carbonyl-O hydrogen bond causes the Lys79 to Thr28 carbonyl-O water-bridge to be less optimal (Fig. S4). Inspection of the structure of the Y46F variant of Hu Cyt*c* [41], shows that the water bridge from the ε-amino group of Lys79 to the Thr28 carbonyl-O is disrupted, in addition to the loss of the Tyr46 hydroxyl to Thr28 carbonyl-O hydrogen bond (Fig. S5). Thus, the Y46F substitution observed in SM Cyt*c* appears to have a general destabilizing effect on the hydrogen bond network connecting the Ω-loops of Cyt*c*.

We also noted differences in anion binding for the two molecules in the asymmetric unit of SM Cyt*c*. Chain B has no chloride bound (Fig. 6A). Chain A has two chlorides bond, one at the N-terminal end of the 60's helix and the other at the N-terminal end of the short 50's helix (Fig. 6B). Both presumably interact with the positive end of the helix dipole of these helices. There are no electrostatic interactions at distances of ~5 Å or less for the Cl^- near the short 50's helix. The presence of these two different molecules in the asymmetric unit of our structure allows comparisons that may aid in understanding the lack of dependence of pK_{app} for the alkaline transition *of E. coli*-expressed SM Cyt*c* on NaCl concentration. Interpretation of the position of surface side chains, necessary for the following analysis, must be approached with caution because often electron density is missing for outer atoms of long side chains at the protein surface and the effects of packing constraints are difficult to assess. The high resolution of the current structure provides a high quality electron density map (Fig. 3). Good electron density is observed for the surface Glu and Asp side

chains discussed below. The surface Lys side chains, discussed below, have good electron density out to at least the γ-carbon. Still, the limitations of the following discussion should be kept in mind.

The Cl^- at the N-terminus of the 60's helix of chain B of SM Cyt*c* forms a triad of close electrostatic interactions with Lys99 and Glu61 (Fig. 6B). Although Glu61 is 6.7 (chain B, with Cl^-) to 7.0 Å (chain A, no Cl^-) from the N-terminal amino group, the binding of Cl^- at the N-terminus of the 60's helix appears to affect the balance of electrostatic interactions around the N-terminal amino group. The main result is a substantial shift in the position of the side chain of Glu89. In the absence of Cl^-, Glu89 is part of a five-residue salt bridge network with the N-terminal amino group, Asp93, Lys5 and Lys87. In the presence of Cl^-, Glu89 forms a three-way salt bridge with Lys87 and Glu90. The change in the position of Lys87 caused by this three-way salt bridge moves the main chain sufficiently that a hydrogen bond between the carbonyl of Lys86 and the side chain of Arg91, present in the absence of Cl^- (Fig. 6A), is broken (Fig. 6B, see also Fig. 6, caption). This small change in turn affects the electrostatic interactions of Glu69. In the absence of Cl^-, Glu69 forms a salt bridge with Lys86 instead of Arg91. The change in the position of Glu69 in the absence of Cl^- places it 5.6 Å from Lys73 (2.1 Å closer than in the presence of Cl^-).

The binding of Cl^- should stabilize the native state of SM Cyt*c*. Since Ω-loop C controls the opening of Ω-loop D in the alkaline transition [14], stabilization of Ω-loop C by Cl^- binding to the short 50's helix should increase the pK_{app} of the alkaline transition as Cl^- concentration increases. However, the increase in the distance of Glu69 from Lys73 when Cl^- binds should decrease the pK_a of the alkaline state ligand, Lys73, which should decrease pK_{app}. These opposing effects of Cl^- binding to SM Cyt*c* may explain the insensitivity of the pK_{app} of *E. coli*-expressed SM Cyt*c* to increasing NaCl concentration.

The electrostatic network mediated by the N-terminal amino group of *E. coli*-expressed SM Cyt*c* in the absence of Cl^-, places Lys73 in a more negative charge environment that would raise its pK_a and thus the pK_{app} of the Lys73-mediated alkaline transition. This effect of the N-terminal amino group could provide an explanation for the higher pK_{app} at low ionic strength observed for *E. coli*-expressed SM Cyt*c* relative to SM Cyt*c* isolated from its natural source with an acetylated N-terminus (Table 4). In the five-residue salt bridge network in Fig. 6A, Glu89 and Asp93 are within 4.4 Å of each other. An acetylated N-terminal amino group could not provide a positive charge to help mitigate the close approach of Glu89 and Asp93. Thus, the position of Glu89 in the five-residue salt bridge network observed in the absence of Cl^- would be expected to be considerably less favorable with an acetylated N-terminal amino group. Thus, an acetylated N-terminus might favor the less negative electrostatic environment for Lys73 (Fig. 6B), depressing its pK_a at lower ionic strength and thus contributing to the lower pK_{app} of the alkaline transition of SM Cyt*c* from its natural source (Table 4).

4. Conclusion

The recent rapid evolution of primate cytochromes *c* has been attributed primarily to co-evolution with cytochrome *c* oxidase [12, 13]. In this study, we have shown that the stability

of the heme crevice may also be affected on different branches of the primate evolutionary tree. This destabilization may have implications for the peroxidase function of Cyt*c* early in apoptosis. Previous work has suggested that the A50E substitution in SM Cyt*c* versus Hu Cyt*c* destabilizes the heme crevice by causing competition for the heme crevice stabilizing hydrogen bond between the ε-amino group of Lys79 and main chain carbonyl-O of residue 47. Our work shows that the primary effect on heme crevice destabilization is due to the Y46F substitution in SM Cyt*c* versus Hu Cyt*c*. Our high resolution structure of SM Cyt*c* suggests that loss of the Tyr46 hydroxyl to Thr28 carbonyl-O hydrogen bond and of a water bridge that connects the ε-amino group of Lys79 to the Thr28 carbonyl-O are the primary structural factors which lead to heme crevice destabilization.

Supplementary Material

Refer to Web version on PubMed Central for supplementary material.

Acknowledgments

This research was supported by National Science Foundation grants, CHE-0910616 and CHE-1306903 (B.E.B.). B.E.B. acknowledges support from CoBRE grant P20GM103546 from NIGMS. The Bruker microflex MALDI-ToF mass spectrometer was purchased with support from NSF Major Research Instrumentation Grant CHE-1039814.

Abbreviations

Cyt*c*	cytochrome *c*
Hu Cyt*c*	Human cytochrome *c*
iso-1-Cyt*c*	yeast iso-1-cytochrome *c*
SM Cyt*c*	spider monkey cytochrome *c*
GdnHCl	guanidine hydrochloride
NSHX	native-state hydrogen-deuterium exchange
pK_{app}	apparent pK_a of the alkaline conformational transition

References

1. Winge DR. Mol. Cell. Biol. 2012; 32:2647–2652. [PubMed: 22586278]
2. Moore GR, Pettigrew GW. Cytochromes *c*: Evolutionary, Structural and Physicochemical Aspects. 1990
3. Olteanu A, Patel CN, Dedmon MM, Kennedy S, Linhoff MW, Minder CM, Potts PR, Deshmukh M, Pielak GJ. Biochem. Biophys. Res. Commun. 2003; 312:733–740. [PubMed: 14680826]
4. Yu T, Wang X, Purring-Koch C, Wei Y, McLendon GL. J. Biol. Chem. 2001; 276:13034–13038. [PubMed: 11112785]
5. Ow YP, Green DR, Hao Z, Mak TW. Nat. Rev. Mol. Cell Biol. 2008; 9:532–542. [PubMed: 18568041]
6. Kagan VE, Bayir HA, Belikova NA, Kapralov O, Tyurina YY, Tyurin VA, Jiang J, Stoyanovsky DA, Wipf P, Kochanek PM, Greenberger JS, Pitt B, Shvedova AA, Borisenko G. Free Radical Biol. Med. 2009; 46:1439–1453. [PubMed: 19285551]

7. Kagan VE, Tyurin VA, Jiang J, Tyurina YY, Ritov VB, Amoscato AA, Osipov AN, Belikova NA, Kapralov AA, Kini V, Vlasova II, Zhao Q, Zou M, Di P, Svistunenko DA, Kurnikov IV, Borisenko GG. Nat. Chem. Biol. 2005; 1:223–232. [PubMed: 16408039]
8. Kagan VE, Chu CT, Tyurina YY, Cheikhi A, Bayira H. Chem. Phys. Lipids. 2014; 179:64–69. [PubMed: 24300280]
9. Tyurina YY, Poloyac SM, Tyurin VA, Kapralov AA, Jiang J, Anthonymuthu TS, Kapralova VI, Vikulina AS, Jung M-Y, Epperly MW, Mohammadyani D, Klein-Seetharaman J, Jackson TC, Kochanek PM, Pitt BR, Greenberger JS, Vladimirov YA, Bayır H, Kagan VE. Nature Chemistry. 2014; 6:542–552.
10. Bandi S, Bowler BE. Biochemistry. 2015; 54:1729–1742. [PubMed: 25671560]
11. McClelland LJ, Mou T-C, Jeakins-Cooley ME, Sprang SR, Bowler BE. Proc. Natl. Acad. Sci. U.S.A. 2014; 111:6648–6653. [PubMed: 24760830]
12. Pierron D, Wildman DE, Hütteman M, Letellier T, Grossman LI. Adv. Exp. Med. Biol. 2012; 748:185–213. [PubMed: 22729859]
13. Pierron D, Opazo JC, Heiske M, Papper Z, Uddin M, Chand G, Wildman DE, Romero R, Goodman M, Grossman LI. PLoS ONE. 2011; 6:e26269. [PubMed: 22028846]
14. Hoang L, Maity H, Krishna MM, Lin Y, Englander SW. J. Mol. Biol. 2003; 331:37–43. [PubMed: 12875834]
15. Osheroff N, Borden D, Koppenol WH, Margoliash E. J. Biol. Chem. 1980; 255:1689–1697. [PubMed: 6243646]
16. Rosell FI, G Mauk A. Biochemistry. 2002; 41:7811–7818. [PubMed: 12056913]
17. Pollock WB, Rosell FI, Twitchett MB, Dumont ME, Mauk AG. Biochemistry. 1998; 37:6124–6131. [PubMed: 9558351]
18. Patel CN, Lind MC, Pielak GJ. Protein Expression Purif. 2001; 22:220–224.
19. Cherney MM, Junior C, Bowler BE. Biochemistry. 2013; 52:837–846. [PubMed: 23311346]
20. Hammack BN, Smith CR, Bowler BE. J. Mol. Biol. 2001; 311:1091–1104. [PubMed: 11531342]
21. Eaton WA, Hochstrasser RM. J. Chem. Phys. 1967; 46:2533–2539. [PubMed: 6039380]
22. Dragomir I, Hagarman A, Wallace C, Schweitzer-Stenner R. Biophys. J. 2007; 92:989–998. [PubMed: 17098790]
23. Otwinowski Z, Minor W. Methods Enzymol. 1997; 276A:307–326.
24. Adams PD, Afonine PV, Bunkóczi G, Chen VB, Davis IW, Echols N, Headd JJ, Hung L-W, Kapral GJ, Grosse-Kunstleve RW, McCoy AJ, Moriarty NW, Oeffner R, Read RJ, Richardson DC, Richardson JS, Terwilliger TC, Zwart PH. Acta Crystallogr., Sect. D: Biol. Crystallogr. 2010; 66:213–221. [PubMed: 20124702]
25. Emsley P, Lohkamp B, Scott WG, Cowtan K. Acta Crystallogr., Sect. D: Biol. Crystallogr. 2010; 66:486–501. [PubMed: 20383002]
26. Krishna MM, Lin Y, Rumbley JN, Englander SW. J. Mol. Biol. 2003; 331:29–36. [PubMed: 12875833]
27. Duncan MG, Williams MD, Bowler BE. Protein Sci. 2009; 18:1155–1164. [PubMed: 19472325]
28. Xu Y, Mayne L, Englander SW. Nat. Struct. Biol. 1998; 5:774–778. [PubMed: 9731770]
29. Krishna MM, Maity H, Rumbley JN, Lin Y, Englander SW. J. Mol. Biol. 2006; 359:1410–1419. [PubMed: 16690080]
30. Mayne L, Englander SW. Protein Sci. 2000; 9:1873–1877. [PubMed: 11106159]
31. Knapp JA, Pace CN. Biochemistry. 1974; 13:1289–1294. [PubMed: 4360785]
32. Godbole S, Hammack B, Bowler BE. J. Mol. Biol. 2000; 296:217–228. [PubMed: 10656828]
33. Cherney MM, Bowler BE. Coord. Chem. Rev. 2011; 255:664–677.
34. Assfalg M, Bertini I, Dolfi A, Turano P, Mauk AG, Rosell FI, Gray HB. J. Am. Chem. Soc. 2003; 125:2913–2922. [PubMed: 12617658]
35. Amacher JF, Zhong F, Lisi GP, Zhu MQ, Alden SL, Hoke KR, Madden DR, Pletneva EV. J. Am. Chem. Soc. 2015; 137:8435–8449. [PubMed: 26038984]
36. Maity H, Rumbley JN, Englander SW. Proteins. 2006; 63:349–355. [PubMed: 16287119]

37. García-Heredia JM, Díaz-Quintana A, Salzano M, Orzáez M, Pérez-Payá E, Teixeira M, Rosa MADl, Díaz-Moreno I. J. Biol. Inorg. Chem. 2011; 16:1155–1168. [PubMed: 21706253]
38. García-Heredia JM, Díaz-Moreno I, Nieto PM, Orzáez M, Kocanis S, Teixeira M, Pérez-Payá E, Díaz-Quintana A, Rosa MADl. Biochim. Biophys. Acta. 2010; 1797:981–993. [PubMed: 20227384]
39. Ying T, Zhong F, Xie J, Feng Y, Wang Z-H, Huang Z-X, Tan X. J. Bioenerg. Biomembr. 2009; 41:251–257. [PubMed: 19593652]
40. Josephs TM, Liptak MD, Hughes G, Lo A, Smith RM, Wilbanks SM, Bren KL, Ledgerwood EC. J. Biol. Inorg. Chem. 2013; 18:289–297. [PubMed: 23334161]
41. Rajagopal BS, Edzuma AN, Hough MA, Blundell KLIM, Kagan VE, Kapralov AA, Fraser LA, Butt JN, Silkstone GG, Wilson MT, Svistunenko DA, Worrall JAR. Biochem. J. 2013; 456:441–452. [PubMed: 24099549]
42. Battistuzzi G, Borsari M, Ranieri A, Sola M. Arch. Biochem. Biophys. 2001; 386:117–122. [PubMed: 11360995]
43. Battistuzzi G, Borsari M, Loschi L, Martinelli A, Sola M. Biochemistry. 1999; 38:7900–7907. [PubMed: 10387031]
44. Martinez RE, Bowler BE. J. Am. Chem. Soc. 2004; 126:6751–6758. [PubMed: 15161303]
45. Verbaro D, Hagarman A, Soffer J, Schweitzer-Stenner R. Biochemistry. 2009; 48:2990–2996. [PubMed: 19222214]
46. Weinkam P, Zimmermann J, Sagle LB, Matsuda S, Dawson PE, Wolynes PG, Romesberg FE. Biochemistry. 2008; 47:13470–13480. [PubMed: 19035653]
47. Battistuzzi G, Borsari M, De Rienzo F, Di Rocco G, Ranieri A, Sola M. Biochemistry. 2007; 46:1694–1702. [PubMed: 17243773]
48. Blouin C, Guillemette JG, Wallace CJA. Biophys. J. 2001; 81:2331–2338. [PubMed: 11566802]
49. Shah R, Schweitzer-Stenner R. Biochemistry. 2008; 47:5250–5257. [PubMed: 18407664]
50. Hagihara Y, Aimoto S, Fink A, Goto Y. J. Mol. Biol. 1993; 231:180–184. [PubMed: 8389881]
51. Nelson CJ, Bowler BE. Biochemistry. 2000; 39:13584–13594. [PubMed: 11063596]
52. Brayer, GD.; Murphy, MEP. Cytochrome *c*. A Multidisciplinary Approach. Scott, RA.; Mauk, AG., editors. Sausalito, California: University Science Books; 1996. p. 103-166.
53. Bushnell GW, Louie GV, Brayer GD. J. Mol. Biol. 1990; 214:585–595. [PubMed: 2166170]
54. Lo TP, Komar-Panucci S, Sherman F, McLendon G, Brayer GD. Biochemistry. 1995; 34:5259–5268. [PubMed: 7711047]
55. Sanishvili R, Volz KW, Westbrook EM, Margoliash E. Structure. 1995; 3:707–717. [PubMed: 8591047]
56. Berghuis AM, Brayer GD. J. Mol. Biol. 1992; 223:959–976. [PubMed: 1311391]
57. Louie GV, Brayer GD. J. Mol. Biol. 1990; 214:527–555. [PubMed: 2166169]

Highlights

- The rapid evolution of primate cytochromes *c* affects heme crevice stability
- The heme crevice stability of spider monkey and human cytochrome *c* is compared
- The Y46F substitution is the primary destabilizer of the heme crevice
- A 1.15 Å resolution structure of spider monkey cytochrome *c* is presented
- The Y46F substitution disrupts a hydrogen bond network connecting 3 surface Ω-loops

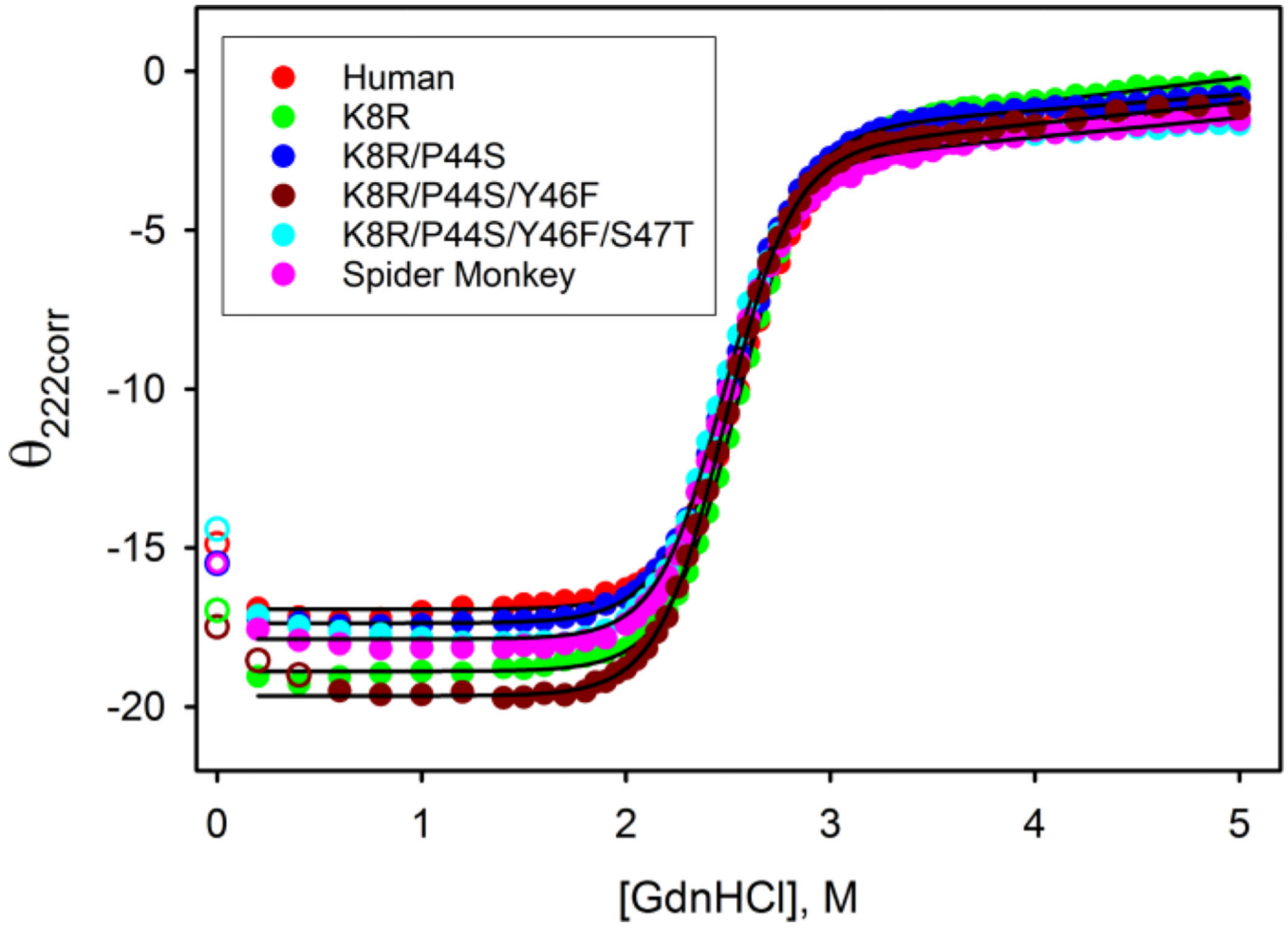

Fig. 1.

Observed changes in corrected ellipticity, $\theta_{222corr}$, as a function of GdnHCl concentration for Hu Cyt*c*, SM Cyt*c* and the set of variants required to convert Hu Cyt*c* into SM Cyt*c*. The solid lines are fits to Eq. (1) in section 2.4 of the Experimentals. Parameters from the fits to Eq. (1) are collected in Table 2. All data were obtained at 25 °C in 20 mM Tris, pH 7, 40 mM NaCl.

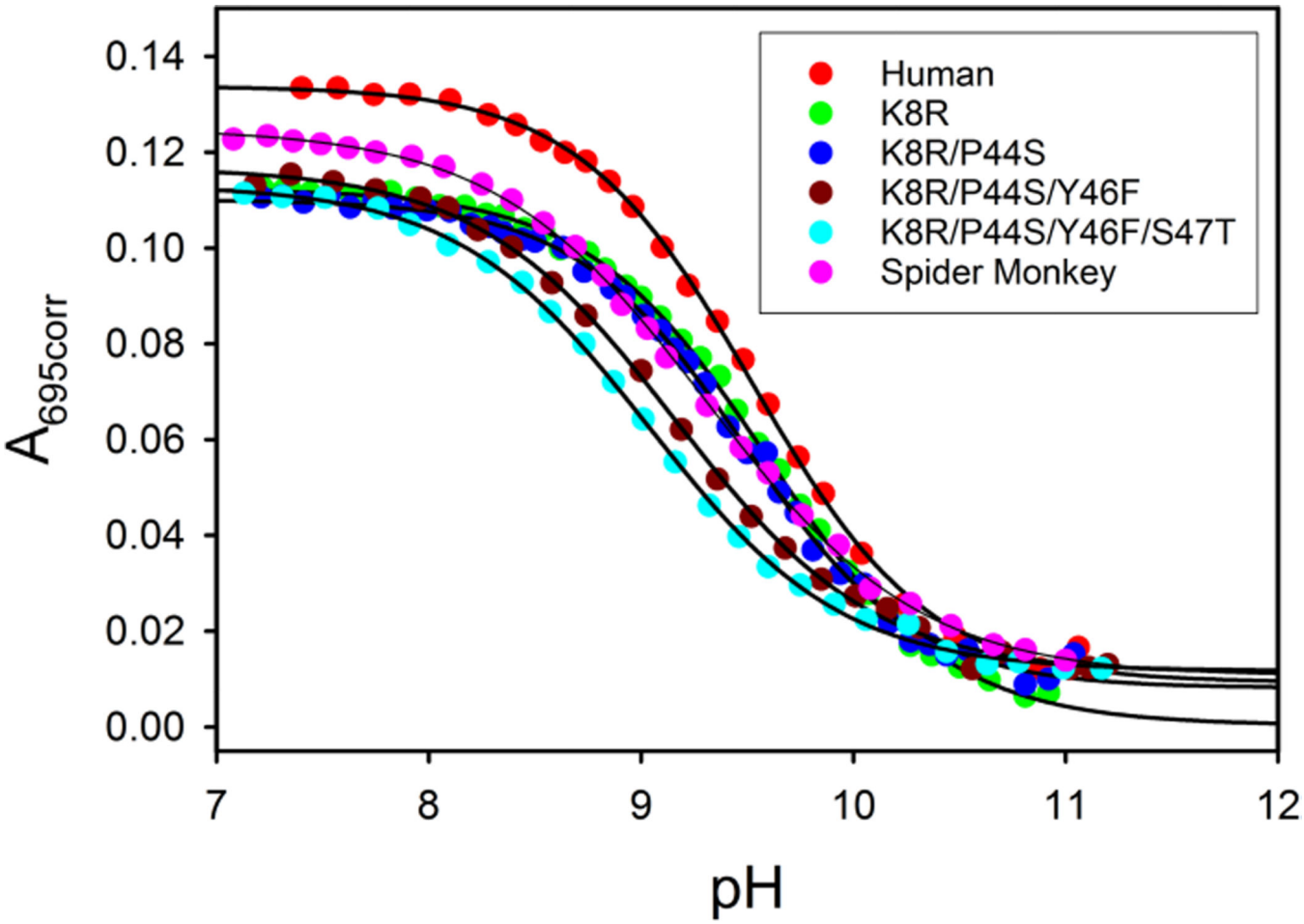

Fig. 2.

Alkaline conformational transition for Hu Cyt*c*, SM Cyt*c* and variants used to convert Hu to SM Cyt*c*. Plots of $A_{695corr}$ versus pH are fit to Eq. (2) in the Experimental (solid curves). Parameters from the fits to Eq. (2) are collected in Table 3. Data were obtained in 100 mM NaCl at ~200 μM protein concentration and at 23 ± 1 °C.

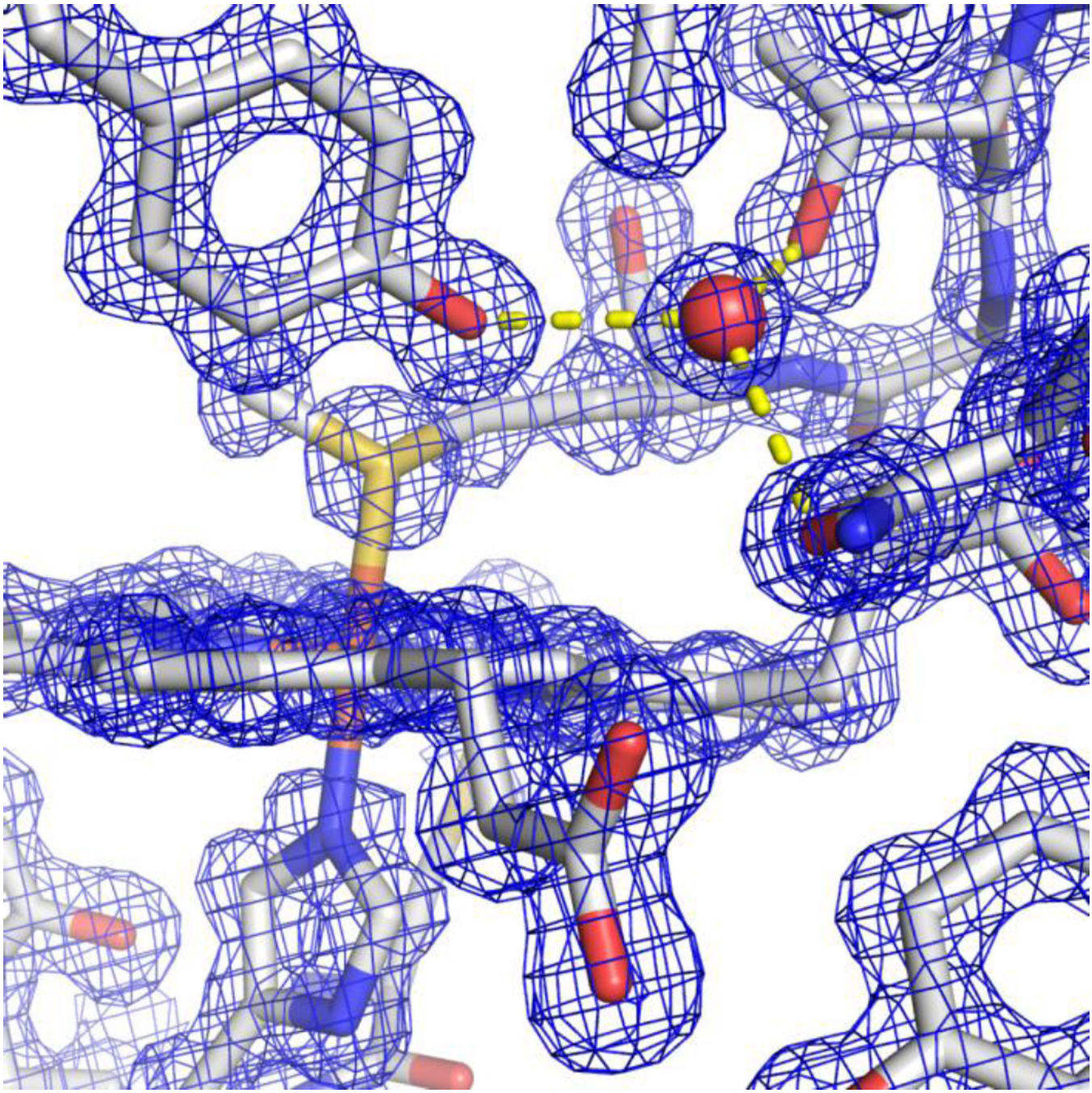

Fig. 3.

Electron density around the heme of chain B of SM Cyt*c* (pdb code: 5DFS) showing buried water (W 332 of chain B) with hydrogen bonds (yellow dashed lines) to the −OH of Tyr67 (2.78 Å), the side chain hydroxyl of Thr78 (2.67 Å) and the carbonyl of the primary amide side chain of Asn52 (2.72 Å).

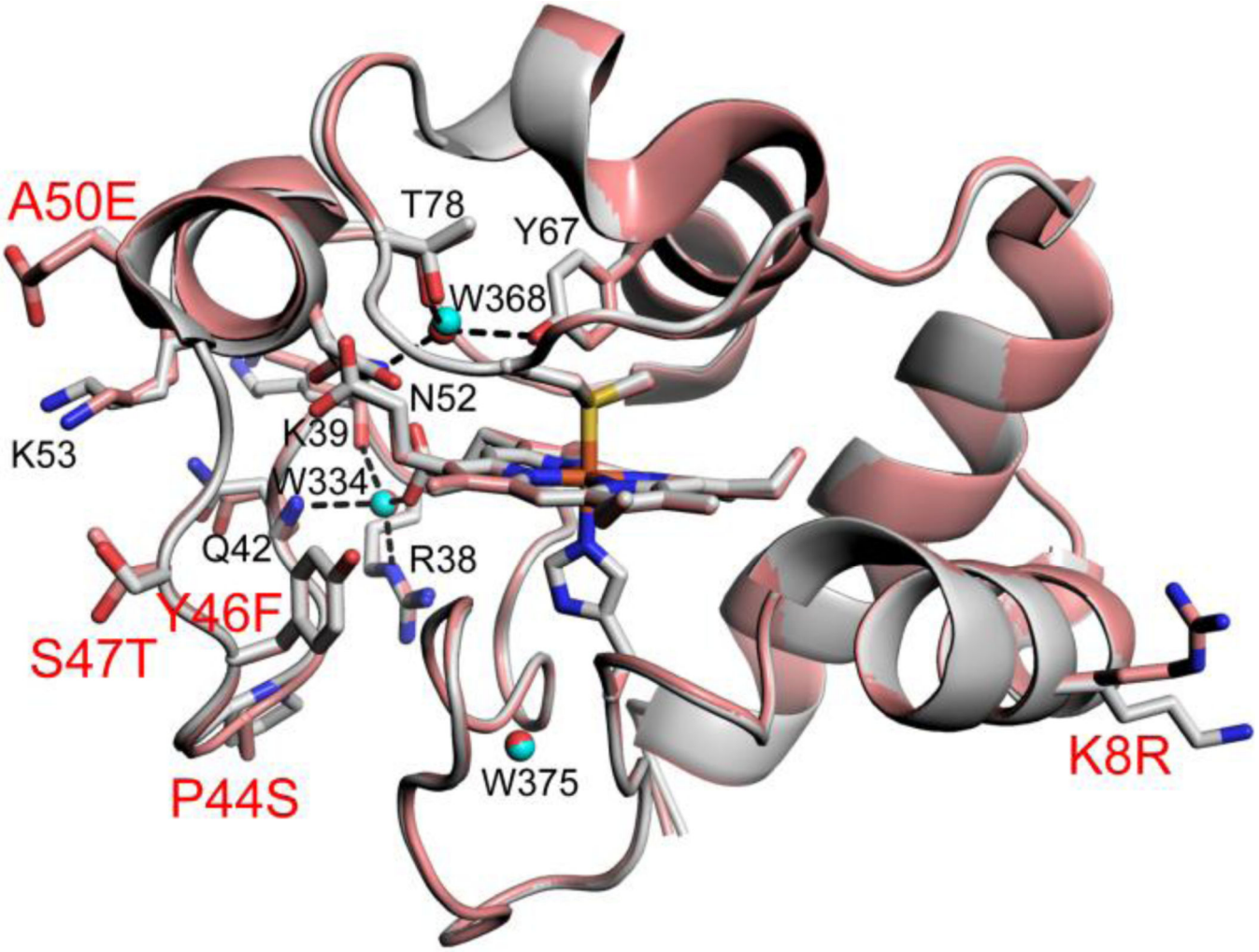

Fig. 4.

Overlay of chain A of Hu Cyt*c* (gray, pdb code: 3ZCF, [41]) with chain A of SM Cyt*c* (salmon, pdb code: 5DFS) showing the five side chain substitutions (stick models with red labels, for Lys8 of Hu Cyt*c*, only one of two fitted side chain rotamers is shown) and the three buried water molecules (cyan spheres for Hu Cyt*c*, red spheres for SM Cyt*c*). The heme and the His18 and Met80 ligands and the side chains of Arg 38, Lys39, Gln42, Asn52, Lys53, Tyr67 and Thr78 are also shown as stick models (black labels). Buried waters are denoted with numbering from the pdb file for chain A of SM Cyt*c* (black labels). Hydrogen bonds from the buried water (W 368) to Tyr67 (2.84 Å), Thr78 (2.80 Å) and Asn52 (3.03 Å) and buried water (W334) to Arg38-δN (2.91 Å), Lys39 carbonyl-O (2.70 Å), Gln42 amide-NH (3.03 Å), and heme propionate A (2.66 Å), are shown with black dashed lines.

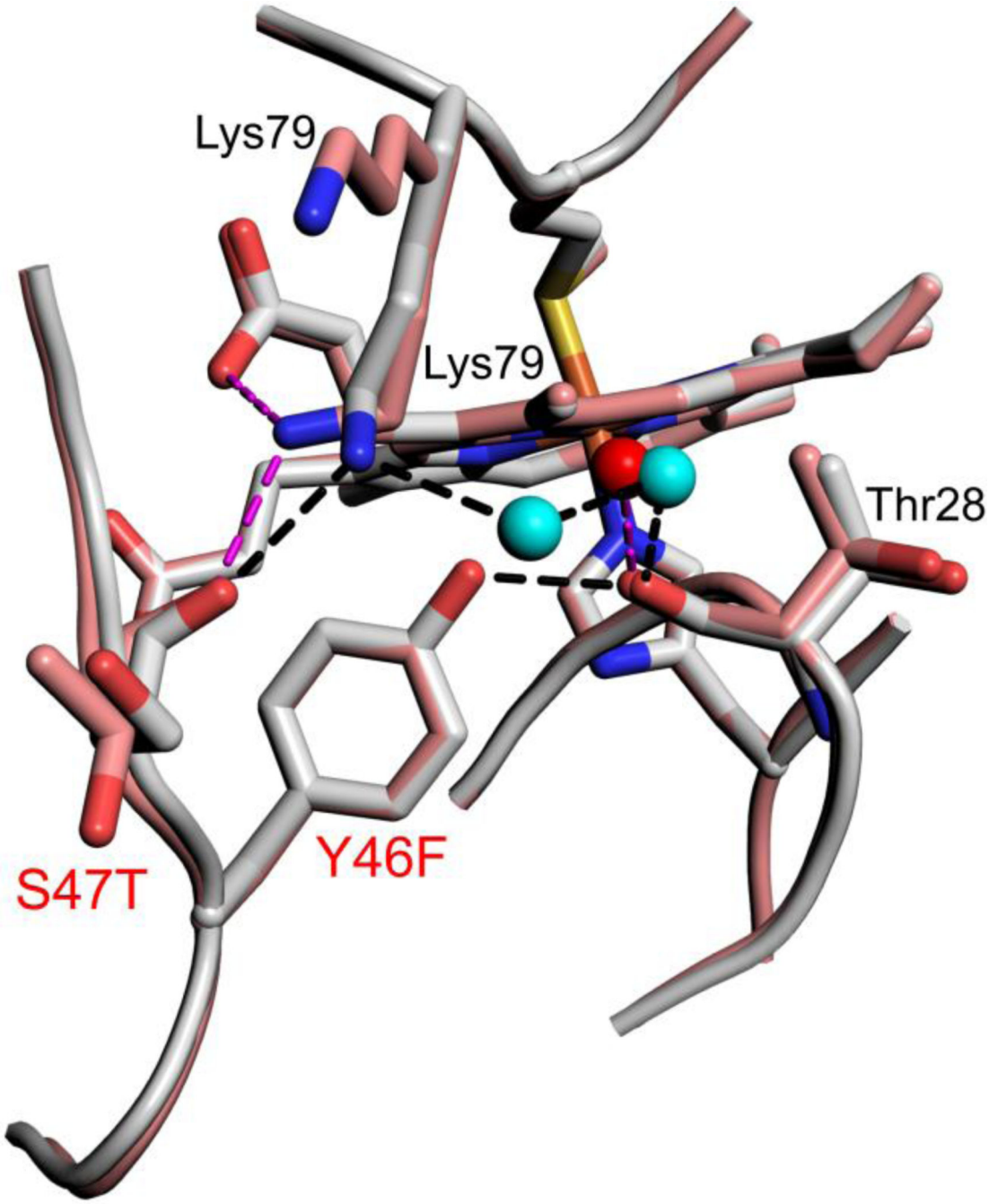

Fig. 5.

Close-up of changes in the hydrogen bond network around position 46 for Hu Cyt*c* (Tyr 46, gray, chain A, pdb code: 3ZCF, [41]) and SM Cyt*c* (Phe46, salmon, chain A, pdb code: 5DFS). Sites of sequence substitutions are labeled red. Other residues involved in the hydrogen bond network have black labels. Both positions of Lys79 in SM Cyt*c* are labeled. Waters in the hydrogen bond network are shown as cyan (Hu Cyt*c*) and red (SM Cyt*c*) spheres. Hydrogen bonds (black dashed lines) for Hu Cyt*c* have the following lengths: Lys79 εN to Ser47 carbonyl-O, 2.84 Å; Lys79 εN to water 2100, 2.76 Å; W2100 to W2043,

2.63 Å; W2043 to Thr28 carbonyl-O, 2.74 Å; Tyr46-OH to Thr28 carbonyl-O, 2.63 Å. Hydrogen bonds (magenta dashed lines) for SM Cyt*c* have the following lengths: Lys79 εN to Thr47 carbonyl-O, 2.76 Å; Lys79 εN to heme propionate D, 3.05 Å; water 362 to Thr28 carbonyl-O, 2.79 Å.

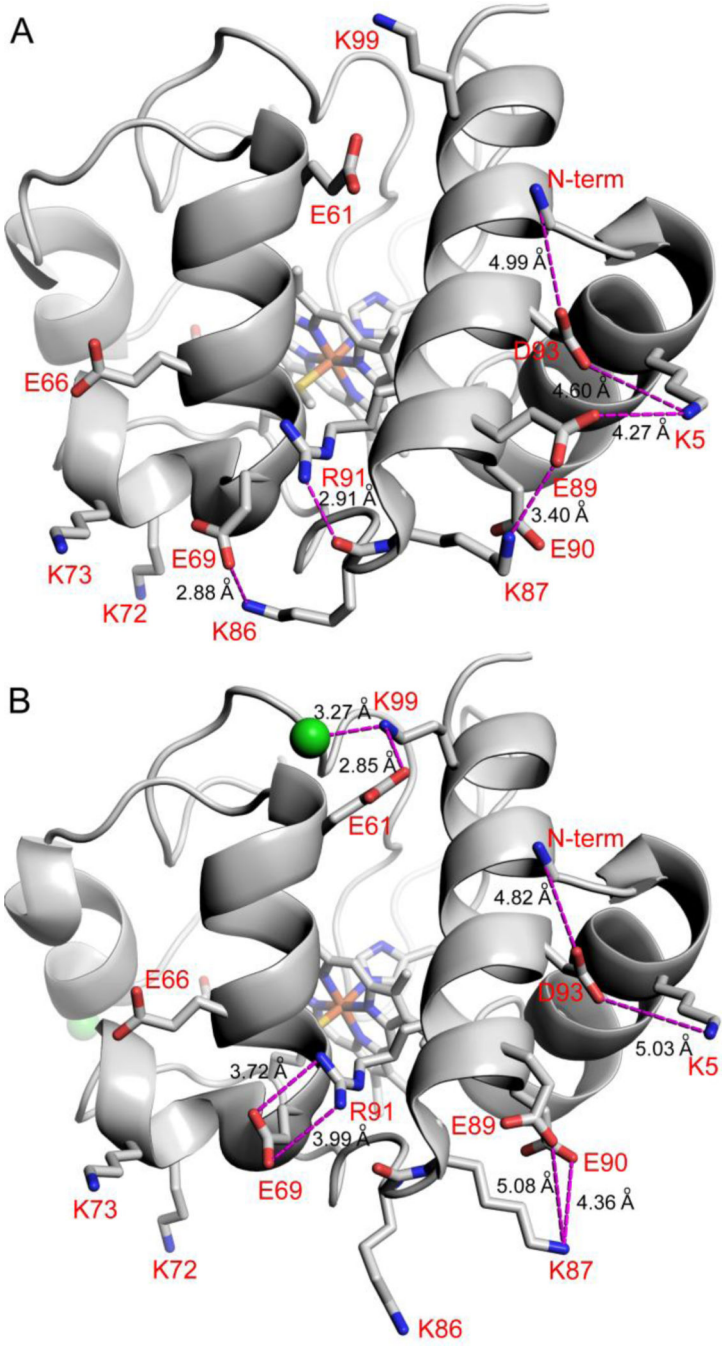

Fig. 6.

Effect of Cl^- binding on electrostatic networks in SM Cyt*c*. (A) Molecule B of SM Cyt*c* (pdb code: 5DFS) showing electrostatic contacts (magenta dashed lines) of ~5 Å or less (distances given in black type) in the absence of Cl^- binding. The dominant conformer (63% occupancy) of Arg91 is shown. The other conformer of Arg91 forms a shorter hydrogen bond of 2.72 Å to the main chain carbonyl of Lys86. (B) Molecule A of SM Cyt*c* (pdb code: 5DFS) showing electrostatic contacts (magenta dashed lines) of ~5 Å or less (distances given in black type) in the presence of Cl^- binding. Cl^- ions are shown as green spheres. The

dominant conformer of Arg91 (83% occupancy) is shown. The minor conformer of Arg91 forms a 2.78 Å hydrogen bond with the main chain carbonyl of Lys86. In both panels residues are labeled in red using one letter amino acids abbreviations and the N-terminal amino group is labeled N-term.

Table 1

X-ray crystallography data collection and refinement statistics.

Beamline	14.1
Wavelength (Å)	1.22
Resolution range (Å)	15.0 – 1.15 (1.19 – 1.15)[a]
Space group	P 2_1
Unit cell dimensions	
a, b, c (Å)	31.5, 42.7, 65.7
α, β, γ (°)	90, 94.5, 90
Total reflections	172044
Unique reflections	62439 (6168)
Multiplicity	2.8 (2.7)[a]
Completeness (%)	97.8 (97.6)[a]
Mean I/σ(I)	15.4 (2.05)[a]
Wilson B-factor	9.30
R_{sym}[b]	0.065 (0.615)[a]
Refinement	
R_{work}[c]	0.159 (0.241)[a]
R_{free}[c]	0.182 (0.249)[a]
Number of total atoms	2099
protein molecule	1679
Ligands	112
Water	308
Total protein residues	208
RMS (bonds, Å)	0.018
RMS (angles, °)	1.64
Ramachandran favored (%)[d]	98
Rotamer outliers (%)	0
Average B-factor	14.50
macromolecules	13.10
Ligands	11.10
Solvent	23.40

[a] Data for highest resolution shell are given in brackets.

[b] $R_{sym} = \sum hkl \sum i \mid I_i(hkl) - \langle I(hkl) \rangle \mid / \sum hkl \sum i I_i(hkl)$ where $I_i(hkl)$ is the i^{th} observation of the intensity of the reflection *hkl*.

[c] $R_{work} = \sum hkl \mid\mid F_{obs}\mid - \mid F_{calc}\mid\mid / \sum hkl \mid F_{obs}\mid$, where F_{obs} and F_{calc} are the observed and calculated structure-factor amplitudes for each reflection *hkl*. R_{free} was calculated with 6% of the diffraction data that were selected randomly and excluded from refinement.

[d] Calculated using MolProbity (Chen et al., 2010).

Table 2

Global stability parameters from GdnHCl denaturation of Cyt*c* variants at 25 °C and pH 7.

Variant	$\Delta G_u°(H_2O)$	*m*	C_m
Human	8.9 ± 0.2	3.51 ± 0.06	2.54 ± 0.01
K8R	9.0 ± 0.1	3.48 ± 0.04	2.58 ± 0.04
K8R/P44S	8.8 ± 0.2	3.52 ± 0.11	2.51 ± 0.02
K8R/P44S/Y46F	8.7 ± 0.2	3.44 ± 0.17	2.52 ± 0.06
K8R/P44S/Y46F/S47T	9.0 ± 0.1	3.66 ± 0.03	2.45 ± 0.01
K8R/P44S/Y46F/S47T/A50E (Spider Monkey)	8.7 ± 0.4	3.49 ± 0.19	2.48 ± 0.02
Equine[a]	7.27	3.01	2.42
Bovine[a]	8.38	3.19	2.62
Yeast[b]	5.77 ± 0.4	5.11 ± 0.36	1.13 ± 0.02

[a] At 25 °C and pH 6.5. Data are from Ref [31]

[b] At 25 °C and pH 7.5. See ref. [32].

Table 3

Parameters for the alkaline conformational transition of Cyt*c* at 23 ± 1 °C in 0.1 M NaCl solution.

Variant	pK_{app}	*n*
Human	9.54 ± 0.03	1.03 ± 0.02
K8R	9.63 ± 0.07	1.02 ± 0.06
K8R/P44S	9.51 ± 0.05	1.06 ± 0.06
K8R/P44S/Y46F	9.15 ± 0.02	0.93 ± 0.02
K8R/P44S/Y46F/S47T	9.05 ± 0.01	0.90 ± 0.05
Spider Monkey	9.32 ± 0.03	0.87 ± 0.01

Table 4

Parameters for the alkaline conformational transition of SM Cyt*c* at 23 ± 1 °C as a function of solution ionic strength.

Ionic Strength[a]	Spider Monkey (*E*. Coli-expressed)		Spider Monkey (Natural Source)[b]
	pK_{app}	*n*	pK_{app}
10 mM[c]	9.21 ± 0.03	0.79 ± 0.04	8.70 ± 0.05
50 mM	9.15 ± 0.05	0.78 ± 0.01	_
250 mM	9.22 ± 0.02	0.89 ± 0.05	9.30 ± 0.05

[a] Ionic strength adjusted with NaCl in the presence of 10 mM Tris acetate

[b] Values from ref. [15]. Values of *n* not reported individually, a range of 0.8 to 1.1 was indicated. 10 mM value was obtained in the presence of Tris acetate. Ionic strength for 250 mM was adjusted with sodium acetate.

[c] 10 mM Tris acetate, no NaCl added.